IEEE Access
Multidisciplinary ⋮ Rapid Review ⋮ Open Access Journal

Received September 2, 2020, accepted September 22, 2020, date of publication September 25, 2020, date of current version October 7, 2020.

Digital Object Identifier 10.1109/ACCESS.2020.3026917

3D Smith Chart Constant Quality Factor Semi-Circles Contours for Positive and Negative Resistance Circuits

VICTOR ASAVEI[1], (Member, IEEE), ANDREI A. MULLER[2], (Senior Member, IEEE), ESTHER SANABRIA-CODESAL[3], ALIN MOLDOVEANU[1], (Member, IEEE), AND ADRIAN M. IONESCU[2], (Fellow, IEEE)

[1]Department of Computer Science and Engineering, Faculty of Automatic Control and Computers, University Politehnica of Bucharest, 060042 Bucharest, Romania
[2]Nanoelectronic Devices Laboratory (NanoLab), École Polytechnique Fédérale de Lausanne (EPFL), 1015 Lausanne, Switzerland
[3]Departamento de Matemática Aplicada, Universitat Politècnica de València, 46022 Valencia, Spain

Corresponding author: Andrei A. Muller (andrei.muller@epfl.ch)

This work was supported in part by the Phase-Change Switch Fet-Open H2020 Grant 737109, in part by the DGC Grant 2018-094889-B-100, in part by the Competitiveness Operational Program 2014-2020, in part by the Action 1.1.3: Creating synergies with RDI actions of the EU's HORIZON 2020 Framework Program and other international RDI programs, under MySMIS Code 108792, and in part by the Acronym Project "UPB4H" under Contract 250/11.05.2020.

ABSTRACT The article firstly proves that the constant quality factor (Q) contours for passive circuits, while represented on a 2D Smith chart, form circle arcs on a coaxal circle family. Furthermore, these circle arcs represent semi-circles families in the north hemisphere while represented on a 3D Smith chart. On the contrary, it then shows that, the constant Q contours for active circuits with negative resistance form complementary circle arcs on the same family of coaxal circles in the exterior of the 2D Smith chart. Moreover, we reveal that these constant Q contours represent complementary semi-circles in the south hemisphere while represented on the 3D Smith chart for negative resistance circuits. The constant Q semi-circles implementation in the 3D Smith chart computer aided design (CAD) tool is then successfully used to evaluate the quality factor variations of newly fabricated Vanadium dioxide inductors, directly from their reflection coefficient, as the temperature is increased from room temperature to 50 degrees Celsius (°C). Thus, a direct multi-parameter frequency dependent analysis is proposed including Q, inductance and reflection coefficient for inductors. Then, quality factor direct evaluation is used for two tunnel diode small signal equivalent circuits analysis, allowing for the first time the direct analysis of the Q and input impedance on a 3D Smith chart representation of a circuit, while including negative resistance.

INDEX TERMS Quality factor, Smith chart, microwave circuits, negative resistance, contour plots, CAD, phase change materials.

I. INTRODUCTION

The Smith chart [1], [2], which, was invented by Philip Hagar Smith in 1939, has survived the passing of years, becoming an icon of microwave engineering [3]. It is still being used in the design and measurement stage of various radio frequency or microwave range devices [4]–[7], for plotting a variety of frequency dependent parameters.

Constant quality factor (Q) representations on the Smith chart are a visual way to determine the quality factor of various passive microwave circuits, being mostly known in the microwave frequency range community [8]–[17]. These constant Q shapes are often denoted as contours or curves, [8]–[12] but rarely as circles [11].

In this work we first prove that the constant Q curves represent circle arcs mapped on coaxal circle families [18] while providing for the first time (to the best of our knowledge) their equations, i.e. centre-radius-Q dependency.

We go on to prove that these circle arcs represent simple semi-circles on the North hemisphere for all passive circuits, when analysed on the 3D Smith chart computer aided design (CAD) tool [19]–[21]. After displaying the constant Q-arcs

The associate editor coordinating the review of this manuscript and approving it for publication was Kuang Zhang.

for negative resistance circuits, we prove that these represent semi-circles in the South hemisphere.

In order to prove the utility of our CAD implementation, we show that, while grounding the second port of newly fabricated Vanadium dioxide 2-port inductors [22], one may get the Q-frequency dependency directly from the S_{11}-reflection coefficient parameter, thus avoiding classical 2D Q-frequency plots previously employed by us [22], [23] or other authors [24], [25], in these type of evaluations. The proposed visualization on the 3D Smith chart proves its effectiveness for passive circuits, especially when Qs do not exceed big values [22]–[25], being particularly useful for Vanadium dioxide temperature variations studies on Q - where Q degrades as temperature increases, but potentially applicable in all inductors' frequency dependent Q evaluations. Here we test the temperature dependence of Q for fabricated inductors with VO_2 by sweeping it from 25°C to 50°C - directly from the vector network analyser with the newly developed technique. Further we show the utility of the new CAD implementation for negative resistance circuits and we analyse the quality factor of various tunnel diodes, when negative resistance occurs, and the 2D Smith chart cannot be used anymore.

II. CONSTANT Q SEMI-CIRCLES REPRESENTATION AND APPLICATIONS

A. CONSTANT Q CIRCLE ARCS ON THE 2D SMITH CHART-EQUATIONS

The quality factor of an impedance Z or admittance Y can be defined as (1) [12]–[17], (this is denoted also as nodal quality factor in [15]–[17]) where X represents its reactance, B its susceptance, R resistance and G conductance as defined in (1) where Z and Y can be related through (2). Other authors skip the absolute value sign in (1) [8]–[11], however this doesn't change anything in respect to their geometry, only to the sign labelling convention. Using the sign conventions [12]–[17] (as for example at p.102 in [13]), we do not allow negative Q values for passive circuits with positive resistances.

$$Q = \frac{|X|}{R} = \frac{|B|}{G}; \tag{1}$$

$$Z = \frac{1}{Y} = R + jX = \frac{1}{G + jB} \tag{2}$$

On the other hand, the reflection coefficient of 1- port network (where R_1 is the port resistance, usually 50 Ω) can be defined as:

$$S_{11}(z) = \frac{Z - R_1}{Z + R_1} = \frac{R + jX - R_1}{R + jX + R_1} = \frac{r + jx - 1}{r + jx + 1} = \frac{z-1}{z+1} = \rho_r + j\rho_i \tag{3}$$

where r and x denote the normalized resistance, respectively reactance:

$$r = \frac{R}{R_1}, \quad x = \frac{X}{R_1}, \; z = r + jx \tag{4}$$

and ρ_r and ρ_i denote the real and the imaginary part of the reflection coefficient.

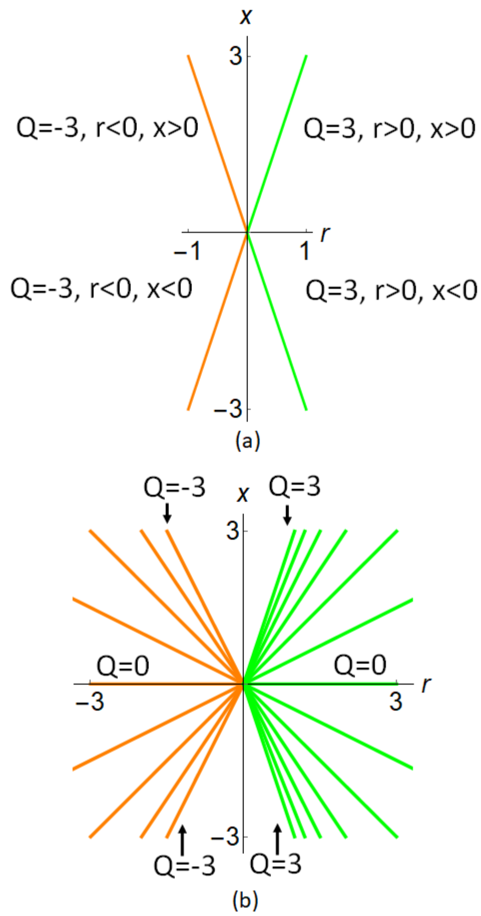

FIGURE 1. Constant Q lines in the z plane a) $|Q| = 3$ radial lines. As r and x are swept from $-\infty$ to ∞, the constant Q lines passing through 0 and infinity b) Various constant Q lines for $-3 \le Q \le 3$.

Based on (1) and (4) one can easily obtain Q as (5).

$$Q = \frac{|x|}{r} \tag{5}$$

If $Q \neq 0$ is constant, we observe that the expression (5) represents radial lines in the normalized impedance (z plane). Fig. 1 (a) shows that for $|Q| = 3$ half-line obtained by the correlation (5) between r and x for this fixed Q while sweeping them. Fig. 1 (b) shows the family of the radial lines obtained for various values of $Q \neq 0$.

Imposing now Q constant and positive in (3) one gets the contours obtained in [8]–[17] irrespective of the presence of the absolute value in (1). However, by using inversive geometry [18], it can be proven that imposing (5) in (3), the set of radial constant Q lines is proven to generate a family of coaxal circles as r and x are swept from $-\infty$ to $+\infty$.

Proof: We know from [18], [19] that any transformation of form (6) represents an inversive transformation mapping always generalized circles (circles or infinite lines) into generalized circles.

$$A(z) = \frac{az + b}{cz + d}; \tag{6a}$$

$$B(z) = \frac{a\bar{z} + b}{c\bar{z} + d} \tag{6b}$$

TABLE 1. Distance between consecutive constant Q circles (Q, Q+1) and reactance axes crossings for $Q \geq 0$.

Q, Q+1 VALUES	DISTANCE	INTERSECTIONS WITH ρ_i $\frac{\pm Q^2}{\sqrt{Q^2+Q\sqrt{1+Q^2}}}$
0,1	0.414	$0, \pm 0.414$
1, 2	0.204	$\pm 0.414, \pm 0.618$
2, 3	0.103	$\pm 0.618, \pm 0.721$
3, 4	0.06	$\pm 0.721, \pm 0.781$
4, 5	0.039	$\pm 0.781, \pm 0.82$
5, 6	0.027	$\pm 0.82, \pm 0.847$
6, 7	0.020	$\pm 0.847, \pm 0.867$
7, 8	0.015	$\pm 0.867, \pm 0.883$
8, 9	0.012	$\pm 0.883, \pm 0.883$
9,10	0,009	$\pm 0.883, \pm 0.905$

Since (3) is a particular case of (6) (Mobius transformation) then, when imposing (5) in (3), the radial lines become generalized circles that passes through the points S_{11} (z = 0) = (−1, 0), S_{11} (z = ∞) = (1, 0).

By matching the real part of (3) to zero, we assert that the image of the points $z = \frac{1}{\sqrt{1+Q^2}} \pm \frac{Q}{\sqrt{1+Q^2}} j$ determine the cutting points with the ρ_i axes, i.e.

$$S_{11}(z = \frac{1}{\sqrt{1+Q^2}} \pm \frac{Q}{\sqrt{1+Q^2}} j) = (0, \frac{\pm Q^2}{\sqrt{Q^2+Q\sqrt{1+Q^2}}}) \tag{7}$$

Then, we obtain a coaxal family of circles that pass through (−1, 0) and (1, 0), and their centers lie on the ρ_i axes with radical axis ρ_r ([26], [27]).

By using the bipolar coordinates ([28]), we obtain that the centre (C) and radius (rad) of this family of circles are:

$$C = \left(0, -\frac{sgn\,(x)}{Q}\right), \quad rad = \sqrt{1+\frac{1}{Q^2}} \tag{8}$$

For $Q > 0$ we obtain circular arcs inside of the Smith Chart as observed seldomly too, as in [11].

For $Q = 0$, we have a circle of infinity radius, i.e. the ρ_r axis. We consider that the distance between two constant Q circle centers is given by the distance between their intersections with the ρ_i axis (7), then this distance between two consecutive circles is given in Table 1. Fig. 2 shows the $Q > 0$ circles arcs.

Computing the distance between two consecutive circles, for negative resistance circuits (with $r \leq 0$ implying $Q \leq 0$) we obtain the results in Table 2 . Displaying now the contours for $Q < 0$, we get the circle arcs in Fig.3. At the limit, $Q = 0$, we have a circle of infinite radius, i.e. the $\boldsymbol{\rho}_r$ axis.

Finally, Fig. 4 displays the family of coaxal circles for $-10 \leq Q \leq 10$ when Q is an integer value.

B. 3D SMITH CHART REPRESENTATION OF CONSTANT Q SEMI-CIRCLES

By using the stereographic projection (9), we can get images of the coaxal circles on the 3D Smith chart located

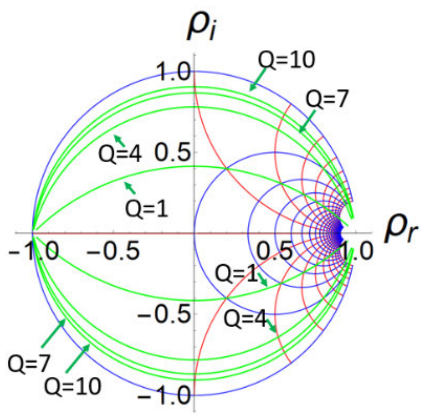

FIGURE 2. Various constant Q circle arcs inside of the Smith chart for $0 \leq Q \leq 10$, with $Q \in N$.

TABLE 2. Distance between consecutive constant Q circles (Q, Q+1) and reactance axes crossings for $Q \leq 0$.

Q, Q+1 VALUES	DISTANCE	INTERSECTIONS WITH ρ_i $\frac{\pm Q^2}{\sqrt{Q^2+Q\sqrt{1+Q^2}}}$
-1, 0	2,41	$0, \pm 2.41$
-2, -1	0.796	$\pm 2.41, \pm 1.61$
-3, -2	0.23	$\pm 1.61, \pm 1.38$
-4, -3	0.106	$\pm 1.38, \pm 1.28$
-5, -4	0.061	$\pm 1.28, \pm 1.22$
-6, -5	0.0393	$\pm 1.22, \pm 1.18$
-7, -6	0.0274	$\pm 1.18, \pm 1.15$
-8, -7	0.0202	$\pm 1.15, \pm 1.13$
-9, - 8	0.0155	$\pm 1.13, \pm 1.12$

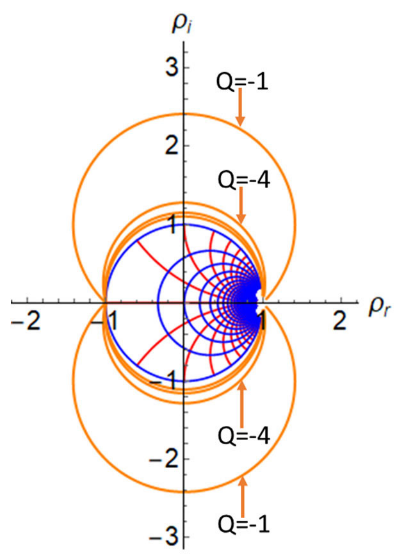

FIGURE 3. Various constant Q circles arcs in the exterior of the Smith chart for Q<0, with $Q \in \mathbb{Z}$.

on the unit space sphere (surface) centered in the origin (0,0,0) [19]–[22].

$$S_{113D}\,(S_{11} = \rho_r + j\rho_i) = \left(\frac{2\rho_r}{1+|\rho|^2}, \frac{2\rho_i}{1+|\rho|^2}, \frac{1-|\rho|^2}{1+|\rho|^2}\right) \tag{9}$$

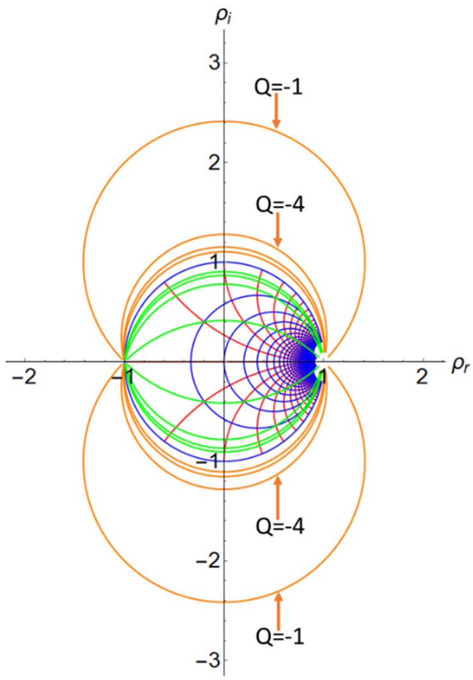

FIGURE 4. Various constant Q circle arcs for $-10 \leq Q \leq 10$, with $Q \in \mathbb{Z}$.

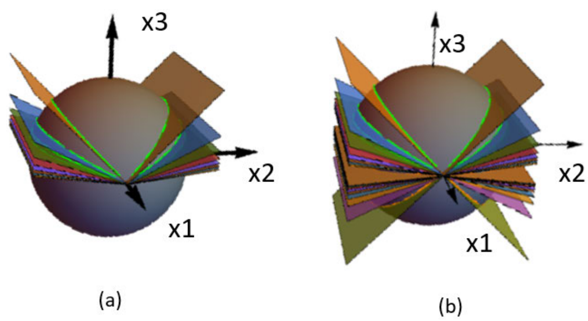

FIGURE 5. Constant Q semi-circles and their fold planes on the 3D Smith chart: (a) for $r > 0$ ($Q > 0$), (b) for $-\infty < r < \infty$, ($-\infty < Q < \infty$).

The coaxal circles become semi-circles on the 3D Smith chart that pass through the points $S_{113D}(-1, 0) = (-1, 0, 0)$, $S_{113D}(1, 0) = (1, 0, 0)$ and $S_{113D}\left(0, \frac{\pm Q^2}{\sqrt{Q^2+Q\sqrt{1+Q^2}}}\right) = (0, \frac{\pm Q}{\sqrt{1+Q^2}}, \frac{1}{\sqrt{1+Q^2}})$.

If we consider (x_1, x_2, x_3) the space coordinates (please see Fig.5), for $Q \neq 0$, these semi-circles are given by the intersection of the 3D Smith chart surface with the fold plane:

$$-2\frac{\operatorname{sgn}(x_2)}{Q}x_2 + 2x_3 = 0, \tag{10}$$

given by the two half-planes corresponding with the positive and negative sign of x_2, respectively, connected by the x_1 coordinate axis.

If $Q = 0$, the corresponding semi-circle passes through the points $(\pm 1, 0, 0)$ and $(0, 0, 1)$, i.e. it is Greenwich meridian. Table 3 summarizes the results generated by (10).

TABLE 3. Constant Q semi-circles on the 3D Smith chart for different values (intersection of the sphere with the Corresponding Surface).

Q	Surface	Comment
0	$x_2 = 0$ (PLANE)	GREENWICH MERIDIAN
-5	$2x_3 + \frac{2}{5}x_2 \operatorname{SGN}(x_2) = 0$ (FOLD PLANE)	SEMI-CIRCLES IN THE SOUTH HEMISPHERE
$+5$	$2x_3 - \frac{2}{5}x_2 \operatorname{SGN}(x_2) = 0$ (FOLD PLANE)	SEMI-CIRCLES IN THE NORTH HEMISPHERE
$\pm\infty$	$x_3 = 0$ (PLANE)	EQUATOR OF THE 3D SMITH CHART

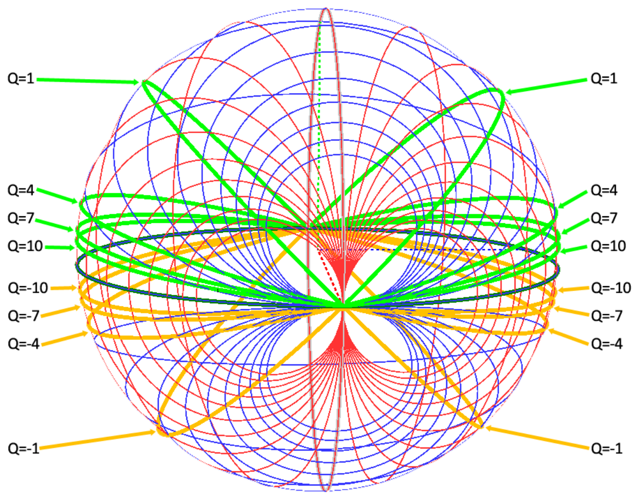

FIGURE 6. Various constant Q semi-circles on the 3D Smith chart for $-10 \leq Q \leq 10$, with $Q \in \mathbb{Z}$.

Fig. 5 shows the constant Q semi-circles on the 3D Smith chart together with the cutting fold planes given by equation (10).

A more detailed view on the rendered 3D Smith chart is given in Fig. 6 for a variety of values of Q.

C. APPLICATIONS IN RECONFIGURABLE INDUCTORS WITH VANADIUM DIOXIDE SWITCHES IN ON/OFF STATE

The quality factor of an inductor is most commonly defined as (11) - by grounding its second port [23]–[25], [29]–[31]. It is usually evaluated until x changes sign and becomes negative. Respectively, we may notice that the imaginary part of the reflection coefficient of a 1-port network can be written as (12) and this becomes zero when x becomes 0. Based on this observation, the zeros of the imaginary part of S_{11} are given by the zeros of x.

$$Q = \frac{Im\left(\frac{1}{Y_{11}}\right)}{Re\left(\frac{1}{Y_{11}}\right)} = \frac{x}{r} \tag{11}$$

$$\rho_i = \frac{2x}{\left(1 + r^2\right) + x^2} \tag{12}$$

Secondly, (11) is identical with (5) under $r > 0$ and $x > 0$ conditions, which are always fulfilled for a passive

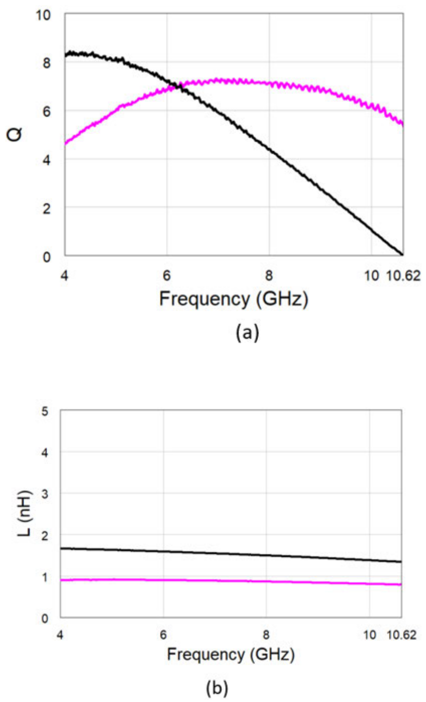

FIGURE 7. On, (pink at 100°C) / off (black at 25°C) extracted frequency dependent parameters of the fabricated inductors measured between 4 GHz and 10.62 GHz: (a) Quality factor (b) Inductance.

inductor below its self-resonant frequency (when it becomes capacitive).

Plotting the 1-port reflection coefficient on the Smith chart delivers the values of the quality factor directly, unlike the 2-port reflection coefficient representations, which are unrelated to it. Displaying the 1-port reflection coefficient (grounding the second port), we can directly detect the quality factors and while using the 3D Smith chart implementation, visualize the extracted inductance and frequency dependency in a concomitant view.

Considering our previous work [22], the inductance can be represented in the 3D space via a homothety over the S_{113D} parameter using (13) where $L_N(\omega)$ represents the normalized extracted inductance.

$$L_{3d}(\omega) = (L_N(\omega) + 1) * \rho_{3D}(j\omega) \tag{13}$$

In [22], the proposed display could not allow for the simultaneous displaying of $L_{3d}(\omega)$, Q and $S_{113D}(\omega)$.

Fig. 7 shows the extracted inductance and Q of the inductors reported in [22] and using VO_2 as switching element using a classical approach. The results are measured at 25 °C (off) and at 100 °C (on).

Let us consider now the representation proposed in the previous section. Fig. 8 (a) displays the S_{113D} of the inductors in on/off states, with the second port grounded, for the same frequency range as in Fig.8. One may directly read the value of the quality factor in each point of them using the proposed CAD implementation, while plotting the convenient constant Q semi-circles. From the 3D rendering it can be visualized that these values are between 7-10 for a wide frequency band,

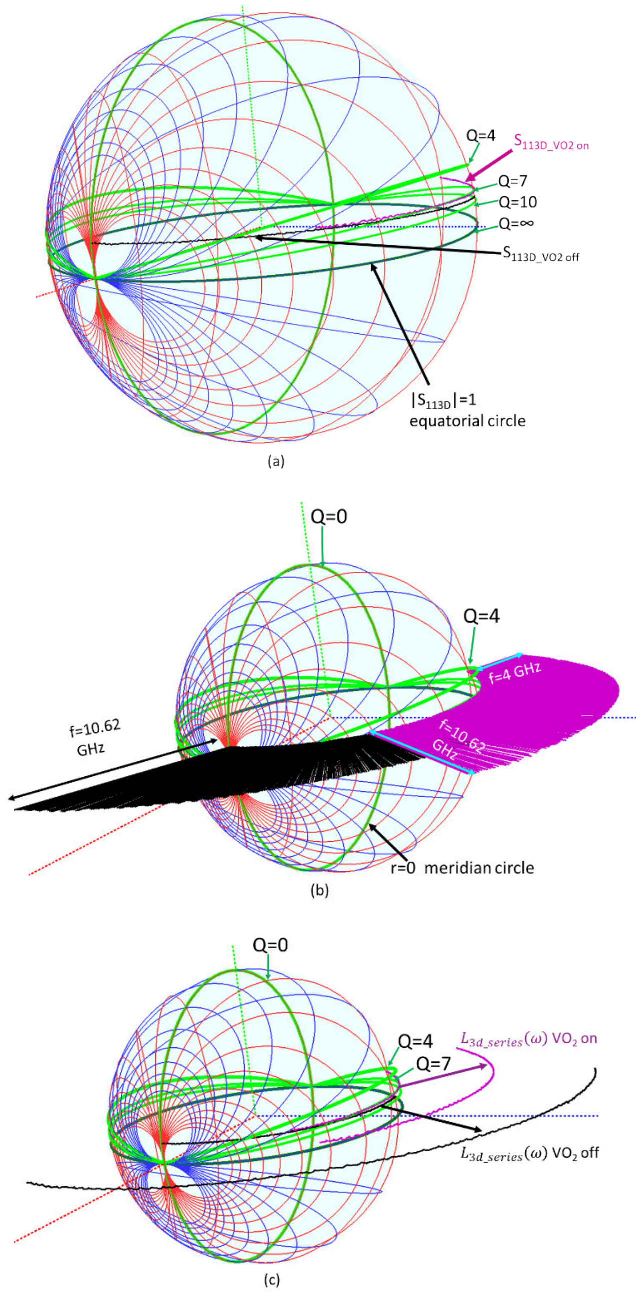

FIGURE 8. On (pink) / off (black) frequency dependent extracted parameters of the fabricated inductors between 4 GHz and 10. 62 GHz on the 3D Smith chart: (a) S_{113D} (b) S_{113D} and frequency visualization (c) S_{113D} and L_{3d}.

while in the case of the off state inductors, these values are decreasing towards 0. For the on state it can be seen clearly that these values do not decrease below 4 for the frequency range displayed. Fig 8 (b) adds the frequency representation proposed in [22] over the previous render, offering their dynamical view as frequency is swept. Fig 8 (c) shows the extracted inductance displayed over them, using a centre projection for each point. The results picture the increased value of the inductance in the off state as in comparison to the one in the on state, while both showing frequency linearity.

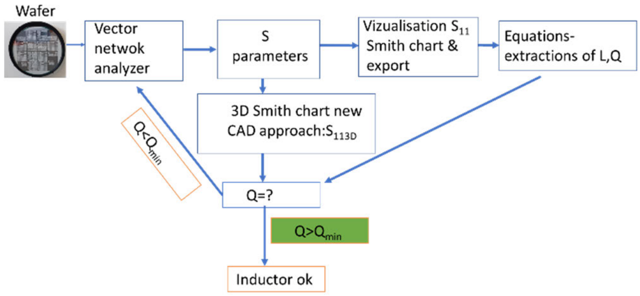

FIGURE 9. Proposed CAD Q evaluation from the S parameters, for a wafer full of inductors requiring Q>Q_{min} on a specific frequency band.

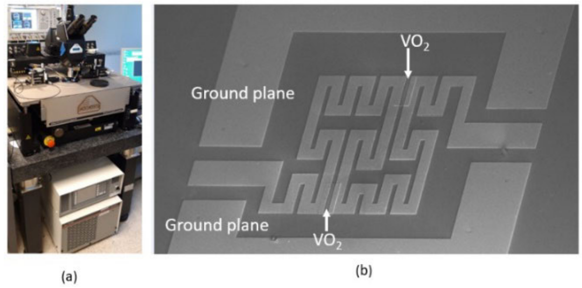

FIGURE 10. (a) Setup for heating the measured wafer: Vector network analyser and a thermo heater below (b) Layout of the inductors [22].

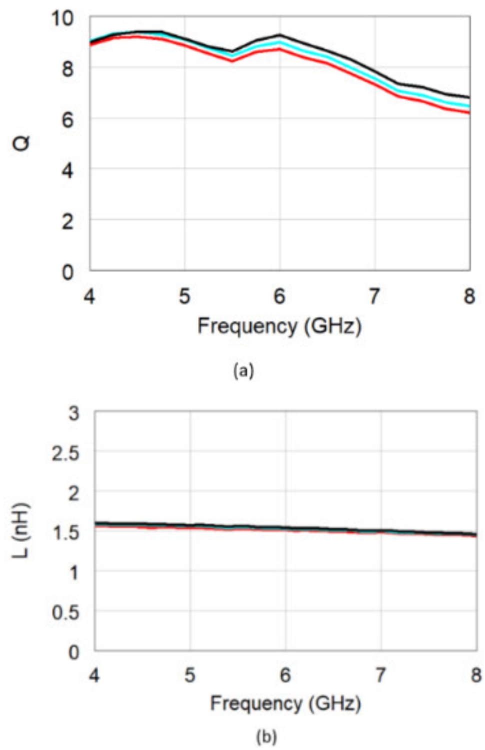

FIGURE 11. Temperature dependence of the inductors RF parameters measured between 4 GHz and 8 GHz while sweeping the temperature from 25 °C (black) to 40 °C (cyan) and 50 °C (red): (a) quality factor (b) extracted inductance.

D. APPLICATIONS IN RECONFIGURABLE INDUCTORS WITH VANADIUM DIOXIDE SWITCHES IN TEMPERATURE SWEEPING

The proposed CAD approach is particularly useful in the case of VO_2 inductors, since these need to be tested at various temperatures, thus a fast detection of a failure, directly from the measured S parameters, would allow for skipping of the testing for the same inductor at a different temperature. On a wafer, that usually has a large number of inductors (ranging from tens to hundreds), the proposed procedure represents a fast tool for detecting quickly failures in the desired expected Q. Fig. 9 summarizes the proposed procedure.

The S parameters can be exported as Touchstone 2-port files and imported directly into the 3D Smith chart application. The application presents a visualisation of the 3D Smith Chart and a wide range of parameters useful in design and analysis, as described in [21], [22]. The application is developed using the Java programming language and for the 3D rendering and interaction with the Riemann sphere the Open Graphics Library (OpenGL) Application Programming Interface (API) is employed. The user can interact with the 3D space in which the Riemann sphere is rendered to manipulate the view of the 3D space and to adjust the parameters of the displayed circuits, as necessary.

In order to test the temperature sensitivity of the Vanadium Dioxide reconfigurable inductors, let us examine a new inductor, based on the design methodology described in [22], but with longer switch length (minimizing losses in off state and increasing them in the on state). The measurement setup is shown in Fig. 10 (a) and includes a thermo chuck, whose temperature is increased up to 50°C. Fig. 10 (b) shows the layout of the inductor, the same as in [22], in this case however with a 2 μm switch length instead of 600 nm as in [22].

Let us now verify the Q frequency dependency while analysing the inductors in the 4-8 GHz and then check the minimum value in this band.

The extracted Q and inductance are displayed in Fig. 11 (a) and (b) on a 2D display. The values of the Q decrease slightly up to 6, while the values of the extracted inductance stay stable with temperature increase-Fig 11(b).

Using the new proposed CAD methodology, we can see in Fig. 12 (a), the $S_{113D}(\omega)$. It can be clearly seen how the Q does not decrease below 6 for none of the analysed temperatures.

Exploiting the frequency dependency display, the dynamics in Fig. 12 (b) can be observed. Fig 12 (c) shows the extracted inductance in 3D - displaying its extremely stable values as temperature increases up to 50°C.

III. NEGATIVE RESISTANCE CIRCUITS

A. FREQUENCY DEPENDENT EXAMPLE

Let us consider the circuit given in Fig. 13, which is the small signal equivalent circuit of a resonant tunnelling diode [32]. These diodes can be used as local oscillators in microwave and millimetre wave frequencies.

Assuming now the values given in [32] for the negative resistance: $R = -120\,\Omega$, shunt capacitance $C = 0.7$pF, while

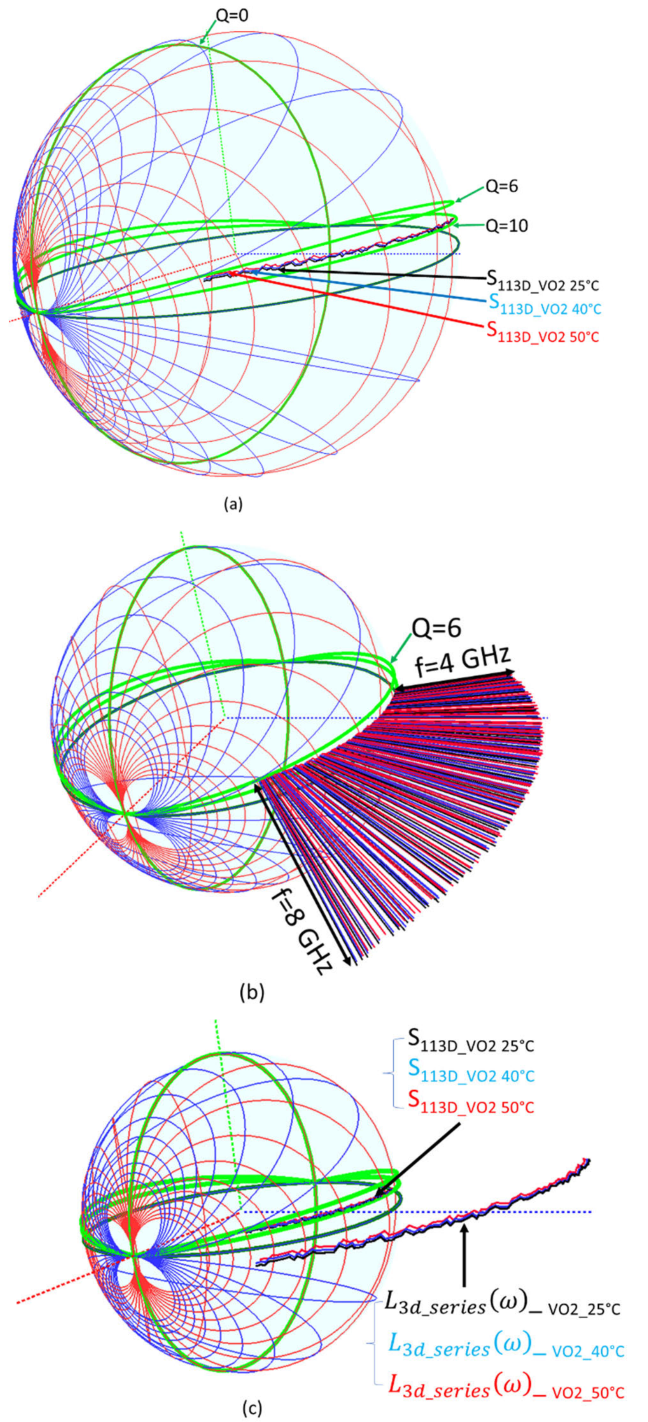

FIGURE 12. Temperature dependence of the inductors parameters measured between 4 GHz and 8 GHz while increasing the temperature from 25 °C (black) to 40 °C (cyan) and 50 °C (red): (a) S_{113D} between the constant Q circles (b) S_{113D} between the constant |Q| circles including frequency dependency-showing their dynamics L_{3D} (c) S_{113D} and L_{3D} displayed simultaneously.

the series resistance $R_S = 3.5\ \Omega$ and the series inductance L=0.5 nH, let us analyse the frequency dependency of its input impedance from its Q in between 5 GHz and 11 GHz. The quality factor of a tunnelling diode can be negative [32],

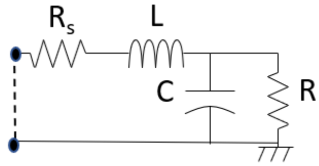

FIGURE 13. Model of the small signal equivalent circuit of a resonant tunnel diode consisting in a negative resistance *R*, shunt capacitance *C* and series resistance R_S and series inductance *L*.

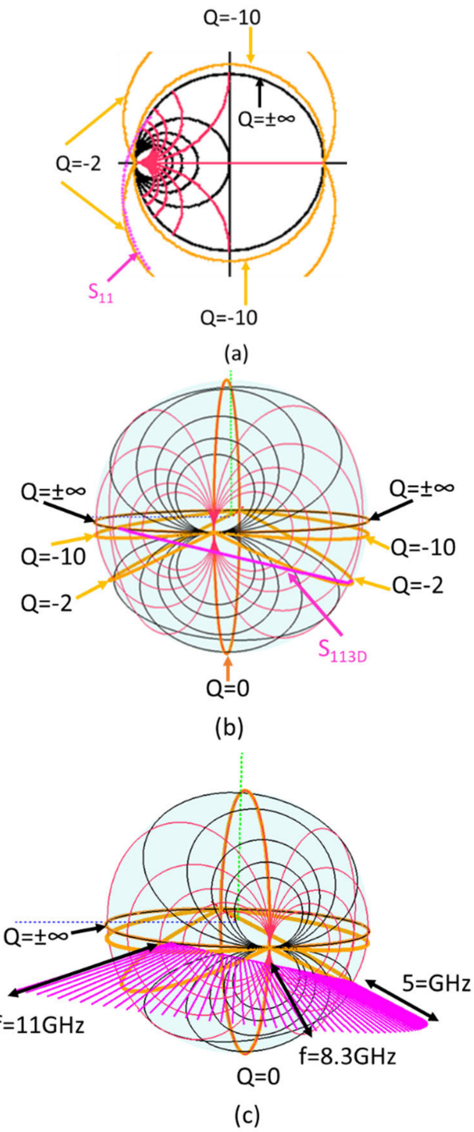

FIGURE 14. Reflection coefficient (pink) of the tunnel diode with a 50 Ω port, for 5 GHz<*f*<11 GHz: (a) in the exterior of the Smith chart (b) on the 3D Smith chart (c) the frequency dependent 3D Smith chart, *Q* = −*2 at 5 GHz, Q=0 at 8.3 GHz, Q=infinity at 11 GHz.*

while keeping the same classical definition. In Fig. 14(a) S_{11} trajectory can only be difficult spotted outside of the Smith chart, crossing constant Q circle arcs. The evolution of the quality factor from values of -2 towards infinity can be seen in Fig. 14 (b)-(c) on a 3D Smith chart rendered with the constant normalized conductance (g) and susceptance (b)

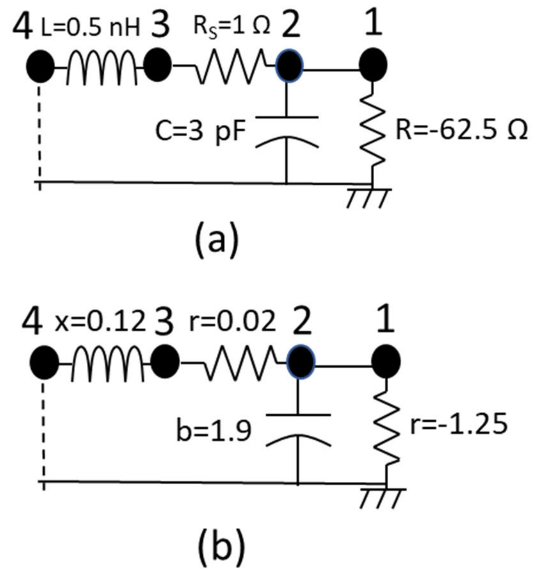

FIGURE 15. Small signal equivalent circuit of the tunnel diode ([2, p. 154]: (a) real values at 2 GHz (b) Normalized to 50 Ω impedance.

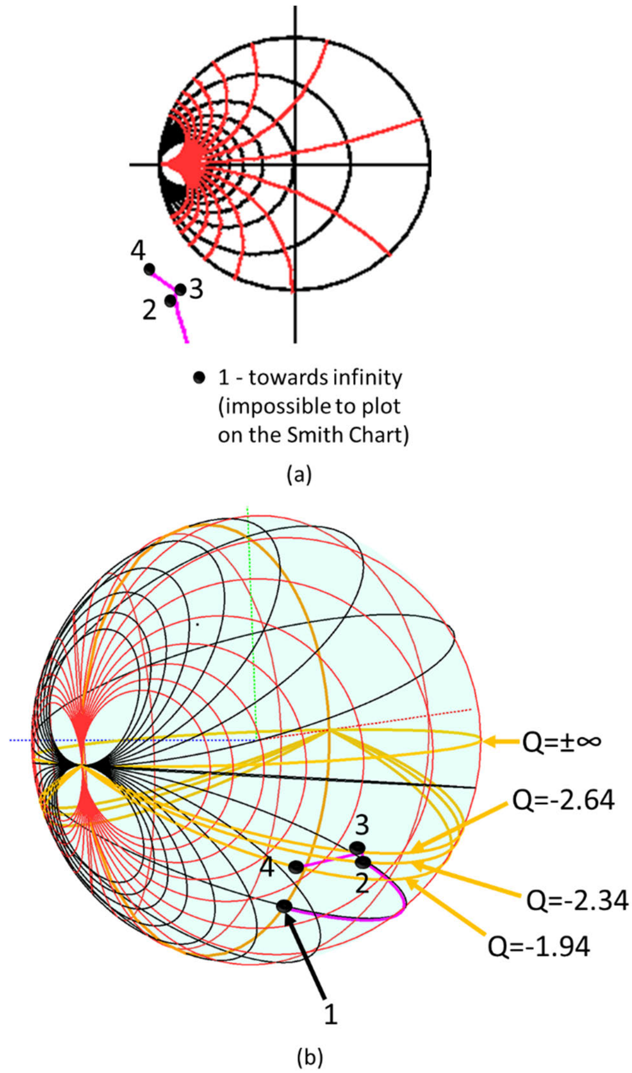

FIGURE 16. Input normalized impedance in the nodes 1-2-3-4 from Fig. 15 (a) on the Smith chart-impossible to plot (b) on the 3D Smith chart.

circles. The values of the normalized input admittance can be checked in each moment along the g and b circles also. While maintaining a negative input resistance, the device behaves capacitive with up to 8.3 GHz when $Q=0$, then from 8.3 GHz the device behaves inductive. Its Q becomes infinite in absolute value at 11 GHz, when its input resistance starts changing sign.

All these evolutions can be easily checked and computed with the 3D Smith chart without the need of further calculations.

B. SINGLE FREQUENCY POINT ANALYSIS

Let us now analyse the tunnel diode small signal equivalent circuit given in Fig. 15 (a) at 2 GHz. ([2, pp 154]. Let us apply the 3D Smith chart implementation to compute the Q and input impedance in the points 1-2-3-4 from Fig. 15 (b) where the normalized values (to a 50 Ω impedance) are given.

Employing a 2D Smith chart in Fig. 16 (a), this would be not possible to further since the negative resistance is thrown towards infinity. On the 3D Smith chart in Fig. 16 (b), we can start from $r = -1.25$, towards South pole, with $Q = 0$ (purely resistive). Thus, in point 1 we can read: $Q = 0$, $r = -1.25$ (or $g = -0.8$). Points1-2: We then move on $g = -0.8$ circle to $b = 1.9$. We can see that we touch the $Q = -2.34$ circle, thus in point 2 we have $g = -0.8$ and $b = 1.9$ (or $x = -0.45$). Points 2-3: we move on the $x = -0.45$ constant circle adding r = 0.02 and get to the point 3 where we intersect the $Q = -2.64$ circle. Thus, we obtain here $r = -0.17$ and $x = -0.45$. Points 3-4: We move on the $r = -0.17$ circle adding the $x = 0.12$ value. In point 4 we can see directly that we cross the $Q = -1.94$ circle thus we obtain $z_{in} = -0.17\text{-}j0.33$, or in un-normalized coordinates: the input impedance becomes: $50^* z_{in} = -8.5\text{-}j16.5$.

We can verify with ease the correctness of the approach by computing the input impedance mathematically. However, the 3D Smith chart implementations allowed us to follow step by step its development in different nodes, with no need of arithmetical manipulations, and, simply by changing the rendering, we were able to read the exact values stepwise.

The appendix shows how the implementation can also be used for a bandstop cell in order to extract the equivalent circuit directly from the S_{11} parameters intersections with constant Q circles.

IV. CONCLUSION

In this article we have proved, for the first time, that the constant Q contours (nodal quality factors) (1) form circle arcs on a family of coaxal circles on the Smith chart. We provided, for the first time (to the best of our knowledge), by means of bipolar equations, their explicit equations in terms of radius, circles centre-Q value relationship, by solving their implicit equations. Further, we have shown while evaluated

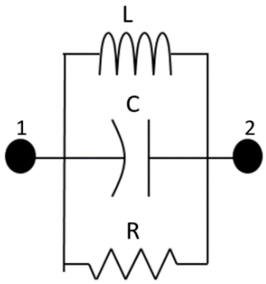

FIGURE 17. Bandstop cell equivalent circuit.

on the 3D Smith chart, the constant Q contours represent semi-circles in the north hemisphere for positive resistance circuits, respectively semi-circles on the south hemisphere for negative resistance circuits, all cantered in 3D Smith chart centre. This simple, compact, and practical circle shaped property has enabled us to use these Q semi-circles directly, in the reflection coefficients plane, for both passive and active circuits, for the direct Q evaluations from measured S parameters.

In the case of Vanadium Dioxide reconfigurable inductors temperature sensitivity analysis: the proposed methodology allowed us the multi-parameter extraction (inductance, Q, reflection coefficient) (Fig. 12) directly from the measured devices, simplifying the extraction procedures-and allowing us a fast evaluation of their performances directly from the measuring setup. In the case of negative resistance circuits, the proposed Q visualization extended the use of constant Q contours for circuits with negative resistance too, impossible on a 2D Smith chart, exemplified here on tunnel diodes small signal equivalent circuits. (Figs. 13-16).

APPENDIX

Let us consider the parallel R, L, C (which can be the equivalent circuit of a bandstop cell) circuit present in Fig. 17. Supposing one would need to determine the values of the elements R, L, C in Fig. 17 that would fit a measured S_{11} of a bandstop cell, whose equivalent circuit is completely determined by Fig. 17: one can use the new frequency dependent Q implementation.

By representing the S_{11} with the second port grounded we obtain Fig. 18.

The input admittance of the bandstop cell (Fig.17) can be computed with (14). At resonance the imaginary part is zero and (15) is fulfilled where ω_0 is the angular resonance frequency, while f_0 the resonance frequency. The input admittance at resonance Y_{110} becomes (16) and Q defined in (13) becomes (17).

$$Y_{11} = \frac{1}{R} + j\left(\omega C - \frac{1}{\omega L}\right) \tag{14}$$

$$\omega_0 = \frac{1}{\sqrt{LC}}, \quad f_0 = \frac{1}{2\pi\sqrt{LC}} \tag{15}$$

$$Y_{110} = \frac{1}{R} \tag{16}$$

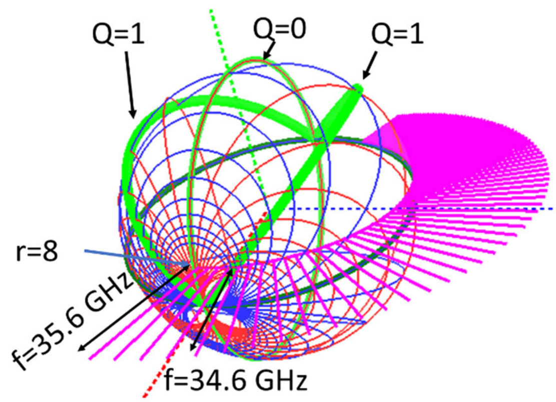

FIGURE 18. S_{11} parameter of the resonant circuit in Fig. 17 with the second port grounded with unknown R,L,C using a 3D Smith chart frequency dependent representation with constant Q semi circles renderings.

$$\frac{Im\left(\frac{1}{Y_{11R}}\right)}{Re\left(\frac{1}{Y_{11R}}\right)} = 0 \tag{17}$$

In Fig. 18 we can easily determine f_0 and R: we check when S_{11} crosses the $Q = 0$ circle and read the values for the frequency and for the normalized resistance. We get $f_0 =$ 35.6 GHz and $r = 8 = R/50$, thus $R = 400\Omega$.

Now let us compute (11) in a general form for the circuit given in Fig. 17:

$$Q = \frac{Im\left(\frac{1}{Y_{11}}\right)}{Re\left(\frac{1}{Y_{11}}\right)} = \frac{R}{\omega L} - RC\omega \tag{18}$$

Imposing now $Q = 1$ we get:

$$\frac{R}{\omega_1 L} - RC\omega_1 = 1 \tag{19}$$

where $\omega_1 = 2^*\pi f_1$ is the angular frequency for which $Q=1$ (and f_1 the frequency for which $Q=1$)

Getting back in Fig. 18 and checking where S_{11} crosses the Q=1 circle we get $f_1 = 34.6$ GHz. Now getting back to (15) and (19) we have:

$$35.6GHz = \frac{1}{2\pi\sqrt{LC}} \tag{20}$$

$$\frac{400}{2\pi * 34.6GHz * L} - 400C * 2\pi * 34.6GHz = 1 \tag{21}$$

Solving using Mathematica [33] numerically (20) and (21) we get one of the solutions: C=0.2 pF and L=0.1 nH. This enabled us to extract the equivalent circuit without any fitting procedure.

ACKNOWLEDGMENT

The authors also want to thank K. Rafter for proof-reading the final version of the paper.

REFERENCES

[1] P. H. Smith, ''Transmission-line calculator,'' *Electron.*, vol. 12, pp. 29–31, Jan. 1939.
[2] P. H. Smith, *Electronic Applications of the Smith Chart*. New York, NY, USA: McGraw-Hill, 1969.
[3] M. S. Gupta, ''Escher's art, Smith chart, and hyperbolic geometry,'' *IEEE Microw. Mag.*, vol. 7, no. 5, pp. 67–76, Oct. 2006.
[4] J. J. Borchardt and T. C. Lapointe, ''U-slot patch antenna principle and design methodology using characteristic mode analysis and coupled mode theory,'' *IEEE Access*, vol. 7, pp. 109375–109385, 2019.
[5] C. F. Goncalves, F. M. Barradas, P. M. Cabral, and J. C. Pedro, ''Switch-based variable length stubs network for PA load sensitivity reduction,'' *IEEE Access*, vol. 7, pp. 152576–152584, 2019.
[6] W. P. Cao, J. Li, W.-B. Ye, and J.-A. Han, ''A 55-65 GHz internal differentially matched silicon power amplifier with spirally folded 1:2 balun,'' *IEEE Access*, vol. 7, pp. 20076–20082, 2019.
[7] H. Sun, X.-W. Zhu, R. Liu, and Z. H. Jiang, ''Mm-wave waveguide traveling-wave power combiner design using an equivalent circuit model,'' *IEEE Access*, vol. 7, pp. 88327–88337, 2019.
[8] W. B. Kuhn and A. P. Boutz, ''Measuring and reporting high quality factors of inductors using vector network analyzers,'' *IEEE Trans. Microw. Theory Techn.*, vol. 58, no. 4, pp. 1046–1055, Apr. 2010.
[9] A. J. Bichler and RF Micro Devices, ''An introduction to broadband impedance transformation for RF power amplifiers,'' *High Freq. Des.*, vol. 8, pp. 34–46, Jan. 2009.
[10] E. Bloch and E. Socher, ''Beyond the smith chart: A universal graphical tool for impedance matching using transformers,'' *IEEE Microw. Mag.*, vol. 15, no. 7, pp. 100–109, Nov. 2014.
[11] J. F. White, *High Frequency Techniques: An Introduction to RF and Microwave Engineering*. Hoboken, NJ, USA: Wiley, 2016.
[12] A. K. Tiwari, ''Smith chart and its applications,'' *Int. J. Electron. Electr. Eng.*, vol. 4, no. 1, pp. 75–94, 2011.
[13] R. Sorrentino and G. Bianchi, *Microwave and RF Engineering*. Hoboken, NJ, USA: Wiley, 2010.
[14] C. Poole and I. Darwazeh, *Microwave Active Circuit Analysis and Design*. London, U.K.: Elsevier, 2016.
[15] F. C. W. Po, E. de Foucauld, D. Morche, P. Vincent, and E. Kerherve, ''A novel method for synthesizing an automatic matching network and its control unit,'' *IEEE Trans. Circuits Syst. I, Reg. Papers*, vol. 58, no. 9, pp. 2225–2236, Sep. 2011, doi: 10.1109/TCSI.2011.2112830.
[16] R. Molavi, S. Mirabbasi, and M. Hashemi, ''A wideband CMOS LNA design approach,'' in *Proc. IEEE Int. Symp. Circuits Syst.*, Kobe, Japan, vol. 5, 2005, pp. 5107–5110, doi: 10.1109/ISCAS.2005.1465783.
[17] B. Xiong, ''Design strategy of tunable matching network and prototype verification,'' *Electron. Lett.*, vol. 54, no. 25, pp. 1425–1426, Dec. 2018, doi: 10.1049/el.2018.6829.
[18] D. A. Brannan, M. F. Esplen, and J. J. Gray, *Geometry*. New York, NY, USA: Cambridge Univ. Press, 2007.
[19] A. A. Muller, P. Soto, D. Dascalu, D. Neculoiu, and V. E. Boria, ''A 3-D smith chart based on the Riemann sphere for active and passive microwave circuits,'' *IEEE Microw. Wireless Compon. Lett.*, vol. 21, no. 6, pp. 286–288, Jun. 2011.
[20] A. A. Muller, A. Moldoveanu, P. Soto, E. Sanabria-Codesal, S. Lucyszyn, V. Asavei, and V. E. Boria, ''Apollonius unilateral transducer constant power gain circles on 3D smith charts,'' *Electron. Lett.*, vol. 50, no. 21, pp. 1531–1533, Oct. 2014.
[21] A. A. Muller, E. Sanabria-Codesal, A. Moldoveanu, V. Asavei, and S. Lucyszyn, ''Extended capabilities of the 3-D smith chart with group delay and resonator quality factor,'' *IEEE Trans. Microw. Theory Techn.*, vol. 65, no. 1, pp. 10–19, Jan. 2017.
[22] A. A. Muller, A. Moldoveanu, V. Asavei, R. A. Khadar, E. Sanabria-Codesal, A. Krammer, M. Fernandez-Bolaños, M. Cavalieri, J. Zhang, E. Casu, A. Schuler, and A. M. Ionescu, ''3D smith charts scattering parameters frequency-dependent orientation analysis and complex-scalar multi-parameter characterization applied to peano reconfigurable vanadium dioxide inductors,'' *Sci. Rep.*, vol. 9, no. 1, pp. 1–15, Dec. 2019.
[23] E. Andrea Casu, A. A. Müller, M. Cavalieri, A. Fumarola, A. M. Ionescu, and M. Fernandez-Bolaños, ''A reconfigurable inductor based on vanadium dioxide insulator-to-metal transition,'' *IEEE Microw. Wireless Compon. Lett.*, vol. 28, no. 9, pp. 795–797, Sep. 2018.
[24] S. Wang, W. Wang, E. Shin, T. Quach, and G. Subramanyam, ''Tunable inductors using vanadium dioxide as the control material,'' *Microw. Opt. Technol. Lett.*, vol. 59, no. 5, pp. 1057–1061, May 2017.
[25] L. Li, W. Wang, E. Shin, and G. Subramanyam, ''Tunable inductors using integrated vanadium dioxide phase change thin films,'' *Adv. Condens. Matter Phys.*, vol. 2018, pp. 1–7, Jan. 2018.
[26] D. Pedoe, *Circles: A Mathematical View*. Memphis, TN, USA: MAA, 1995.
[27] H. S. M. Coxeter and S. L. Greitzer, ''Coaxal circles,'' in *Geometry Revisited*. Washington, DC, USA: Math. Assoc. Amer., 1967, pp. 35–36 and 122.
[28] E. H. Lockwood, ''A book curves,'' in *Bipolar Coordinates*. Cambridge, U.K.: Cambridge Univ. Press, 1967, ch. 25, pp. 186–190.
[29] N. Wainstein and S. Kvatinsky, ''TIME—Tunable inductors using MEmristors,'' *IEEE Trans. Circuits Syst. I, Reg. Papers*, vol. 65, no. 5, pp. 1505–1515, May 2018.
[30] F. Khan, H. Hussein, and M. I. Younis, ''Spring-shaped inductor tuned with a microelectromechanical electrothermal actuator,'' *IEEE Magn. Lett.*, vol. 11, pp. 1–5, 2020.
[31] L. Li, K. Ma, and S. Mou, ''Modeling of new spiral inductor based on substrate integrated suspended line technology,'' *IEEE Trans. Microw. Theory Techn.*, vol. 65, no. 8, pp. 2672–2680, Aug. 2017.
[32] R. Bouregba, O. Vanbesien, L. S. de Pol, and D. Lippens, ''$Al_{0.3}Ga_{0.7}$ As-GaAs microwave resonant tunneling oscillator,'' *Ann. Telecommun.*, vol. 45, pp. 184–191, Mar. 1990. [Online]. Available: https://link.springer.com/article/10.1007/BF02995153
[33] *Wolfram Mathematica Version 12*, 2020.

VICTOR ASAVEI (Member, IEEE) received the Ph.D. degree in computer science and information technology from the University Politehnica of Bucharest, in 2011.

He is currently an Assistant Professor (Lecturer) with the Computer Science and Engineering Department, Faculty of Automatic Control and Computers, University Politehnica of Bucharest. He has coauthored approximately 60 articles and four books in the fields of computer graphics, distributed computing, software engineering, and medical ITs and has participated in numerous national and international research projects. His current teaching and research interests include real time computer graphics and general purpose computing on graphics processing units (GPGPU).

ANDREI A. MULLER (Senior Member, IEEE) was born in Bucharest, Romania. He received the degree in mobile and satellite communications and the Ph.D. degree in microwaves engineering from Politehnica Bucharest. Being an Ex-Marie-Curie Fellow in i-Team, UPV Valencia, Spain, he has been the Scientist of Nanolab, EPFL Lausanne, since September 2017. His current research interests include CAD and smart materials for RF and microwaves engineering. He was a recipient of the Gheorghe Cartianu Prize of the Romanian Academy of Science in 2013 for the article ''A 3D Smith chart Riemann Sphere for Active and Passive Microwave Circuits-IEEE MWCL, 2011." He is an Outstanding Associate Editor of IEEE Access in 2017 and 2018.

ESTHER SANABRIA-CODESAL received the Ph.D. degree in geometry and topology from the University of Valencia, Valencia, Spain, in 2002. She is currently an Associate Professor with the Department of Applied Mathematics, Universitat Politècnica de València, Valencia. Her current research interests include theory of singularities applied to geometry and mathematical modeling based on graphs. She has participated in numerous research projects and conferences.

ALIN MOLDOVEANU (Member, IEEE) received the degree (Hons.) from the Faculty of Automatic Control and Computers, Politehnica University of Bucharest.

He is currently a Professor (teaching software engineering and virtual reality) and the Vice-Dean (in charge of the master studies) with the Faculty of Automatic Control and Computers, Politehnica University of Bucharest. He has been teaching software engineering at bachelor level and virtual and augmented reality at masters, and focusing on applied research in virtual and augmented reality (exploring and applying immersion, sensory substitution, and distorted reality), e-health (assistive and rehabilitative solutions, and prevention of hospital acquired infections), and e-learning and e-culture (mixed-reality campuses and cultural environments). He is the Director or responsible for many national or European research projects in these areas, such as sound of vision, TRAVEE, HAI-OPS, and Lib2Life. List of projects and publications available at: https://cs.pub.ro/index.php/people/userprofile/alin_moldoveanu.

Dr. Moldoveanu's research works received several prestigious prizes, such as the Best "Tech for Society" Horizon 2020 Project, awarded by EC through Innovation Radar, at ICT 2018–received by Sound of Vision, where he acted as a Technical Coordinator and UPB Team responsible.

ADRIAN M. IONESCU (Fellow, IEEE) received the B.S./M.S. degrees from the Polytechnic Institute of Bucharest, Romania, in 1989, and the Ph.D. degree from the National Polytechnic Institute of Grenoble, France, in 1997.

He is currently a Professor with the Ecole Polytechnique Fédérale de Lausanne (EPFL), Switzerland. He held staff or visiting positions at LETI-Commissariat à l'Énergie Atomique, Grenoble, Stanford University, and the Tokyo Institute of Technology. He is the Founder and the Director of the Nanoelectronic Devices Laboratory (Nanolab), EPFL. He has published more than 400 papers in international journals and conference proceedings.

Dr. Ionescu has been an Elected Member of the Swiss Academy of Technical Sciences (SATW) since 2015. He was a recipient of the 2013 IBM Faculty Award and the André Blondel Medal 2009, SEE, Paris, France, for contributions to the progress in electronic engineering sciences. He has served on the International IEEE Electron Devices Meeting, IEEE VLSI, and Transducers technical committees. He was the Technical Program Committee Chair/Co-Chair of the European Solid-State Device Research Conference in 2006 and 2013.